Temporal Notch signaling regulates mucociliary cell fates through Hes-mediated competitive de-repression

Magdalena Maria Brislinger-Engelhardt[1,2,3], Fabian Lorenz[2,5], Maximilian Haas[1,3], Sarah Bowden[1,2,4], Alexia Tasca[1], Clemens Kreutz[2,5], Peter Walentek[1,2,3,4,#]

[1] Department of Medicine IV, University Freiburg Medical Center, Faculty of Medicine, University of Freiburg, Hugstetter Strasse 55, 79106 Freiburg, Germany.
[2] CIBSS Centre for Integrative Biological Signalling Studies, University of Freiburg, Schänzlestrasse 18, 79104 Freiburg, Germany.
[3] SGBM Spemann Graduate School for Biology and Medicine, University of Freiburg, Albertstrasse 19A, 79104 Freiburg, Germany.
[4] IMPRS-IEM International Max Planck Research School of Immunobiology, Epigenetics and Metabolism, Max Planck Institute of Immunobiology and Epigenetics, Stübeweg 51, 79108 Freiburg, Germany.
[5] IMBI Institute of Medical Biometry and Statistics, Institute of Medicine and Medical Center Freiburg, Stefan-Meier Strasse 26, 79104 Freiburg, Germany.
[#] Corresponding author: peter.walentek@medizin.uni-freiburg.de

Abstract:

Tissue functions are determined by the types and ratios of cells present, but little is known about self-organizing principles establishing correct cell type compositions. Mucociliary airway clearance relies on the correct balance between secretory and ciliated cells, which is regulated by Notch signaling across mucociliary systems. Using the airway-like *Xenopus* epidermis, we investigate how cell fates depend on signaling, how signaling levels are controlled, and how Hes transcription factors regulate cell fates. We show that four mucociliary cell types each require different Notch levels and that their specification is initiated sequentially by a temporal Notch gradient. We describe a novel role for Foxi1 in the generation of Delta-expressing multipotent progenitors through Hes7.1. Hes7.1 is a weak repressor of mucociliary genes and overcomes maternal repression by the strong repressor Hes2 to initiate mucociliary development. Increasing Notch signaling then inhibits Hes7.1 and activates first Hes4, then Hes5.10, which selectively repress cell fates. We have uncovered a self-organizing mechanism of mucociliary cell type composition by competitive de-repression of cell fates by a set of differentially acting repressors. Furthermore, we present an *in silico* model of this process with predictive abilities.

Key words:

Xenopus, airway epithelium, development, multi-ciliated cells, mucus, basal cells, mathematical modeling

Introduction:

Tissue functions are determined by morphology and by cell type composition, the types, numbers and ratios of cells present, but little is known about the self-organizing principles that govern the establishment of correct cell type compositions. Mucociliary epithelia line various organs in animals(Walentek, 2021b; Walentek and Quigley, 2017), including the mammalian airways and the epidermis of *Xenopus laevis* embryos, where they provide an innate immune barrier through mucociliary clearance(Dubaissi et al., 2014; Whitsett, 2018). This relies on the correct balance between secretory and ciliated cells, which is varied across organs and adapted to location within an organ(Volckaert and De Langhe, 2014). Alterations in cell type composition are characteristic of airway diseases, such as asthma, chronic obstructive pulmonary disease and cancer(Hogan et al., 2014). Lung diseases are a global health burden, but the development of treatments is impeded by our incomplete understanding of the mechanisms regulating correct mucociliary cell type compositions(Walentek, 2021a). Notch regulation of ciliated and secretory cells was shown to be evolutionarily conserved in mucociliary epithelia across species, and frequently disturbed in human airway diseases(Deblandre et al., 1999; Hogan et al., 2014; Kiyokawa and Morimoto, 2020; Rock et al., 2011; Walentek, 2021a). Despite efforts to unravel how Notch signaling regulates mucociliary patterning, precisely how cell fates depend on signaling levels, how signaling levels are generated, and how signaling is interpreted by cells during fate decisions have remained enigmatic. Here, we show that four mucociliary cell types require different Notch signaling levels for specification. Cell fates are initiated sequentially by a temporal Notch gradient generated by ligand-expressing multipotent progenitors. We describe a novel role of the forkhead-box transcription factor Foxi1 in the generation of multipotent progenitors through the activation of Hes7.1, which is required to overcome a maternally deposited repression system. Further cell fate choices are governed by the integration of Notch signaling levels through additional Hes factors and Hes-independent mechanisms. Finally, we present a mathematical model that recapitulates the establishment of mucociliary cell type composition *in silico*, which can be used to predict critical gaps in our understanding of mucociliary patterning mechanisms in development and disease.

Results:

All mucociliary cell types are specified at distinct Notch levels

In the *Xenopus* embryonic mucociliary epidermis, ionocytes (ISCs) and multi-ciliated cells (MCCs) are specified prior to small secretory cells (SSCs)(Dubaissi et al., 2014; Walentek et al., 2014). Elevated *ΔN-tp63* expression induces mature basal stem cells (BCs) and blocks all other cell fates, terminating cell fate specification(Haas et al., 2019). ISCs and MCCs are generated in low Notch conditions, while secretory cells are induced by Notch activation(Deblandre et al., 1999; Quigley and Kintner, 2017; Quigley et al., 2011; Walentek, 2018). It was proposed that early and late progenitors with different potential generate ISCs/MCCs and SSCs, respectively(Briggs et al., 2018).

Brislinger et al. Figure 1

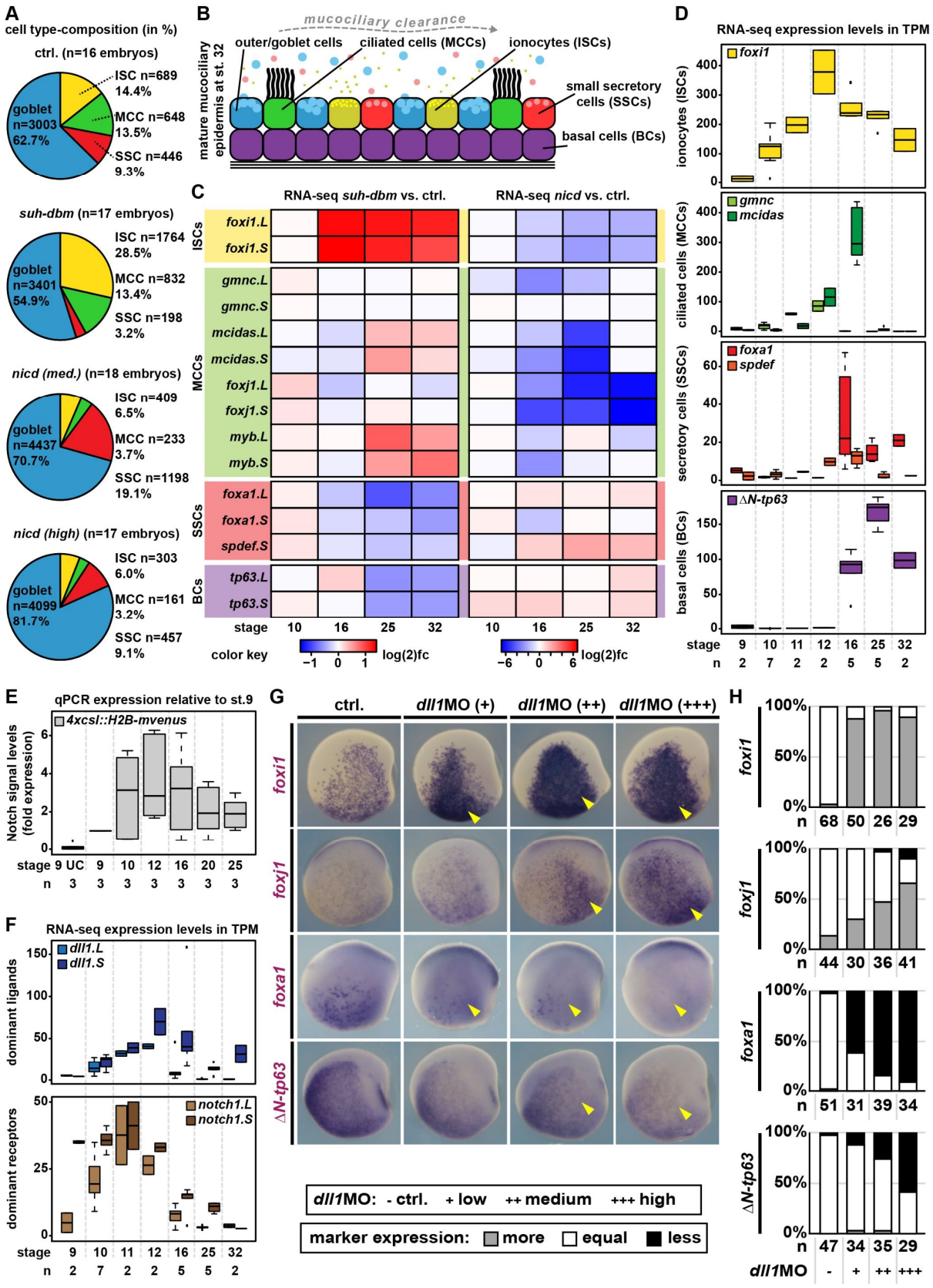

Figure 1: Cell fate specification in response to a temporal Notch gradient

A: Quantification of epidermal cell types after Notch manipulations and immunofluorescent staining at st. 32. **B:** Schematic representation of mucociliary epidermal cell types. **C:** Changes in cell type marker

expression relative to stage-matched controls after manipulation of Notch signaling in *Xenopus* mucociliary organoids (RNA-seq). **D,F:** Expression levels of indicated genes in unmanipulated mucociliary organoids across different stages of development (RNA-seq). **E:** Notch reporter activity in mucociliary organoids relative to *4xcsl::H2B-mvenus* injected st. 9 samples over time (qPCR). **G:** Lateral view, WMISH for indicated transcripts at st. 16/17 in controls and after knockdown of *dll1*. +=low dose, ++=medium dose, +++=high dose. **H:** Quantification of results depicted in G. Expression levels were scored more, equal, less expression on the injected vs. uninjected side.

To elucidate how different Notch signaling levels affect cell type composition, we strongly reduced signaling-induced transcription using *dominant-negative RBPJ* (*suh-dbm*) or overactivated it using *Notch intracellular domain* (*nicd*). At stage (st.) 32, we immuno-stained for cell type markers to analyze control and targeted (=GFP+) specimens by confocal microscopy (**Fig.S1A**)(Walentek, 2018). Notch inhibition increased ISC and decreased SSC numbers, but did not increase MCC numbers (**Fig.1A,B; S1A**). Notch activation lead to a loss of ISCs and MCCs, but intermediate (med.) levels expanded SSC numbers, while high levels suppressed SSCs (**Fig.1A; S1A**).

Using different concentrations of *suh-dbm* or *nicd* mRNA overexpression, we confirmed the graded effects of Notch on cell type composition by whole mount *in situ* hybridization (WMISH) at the end of specification (st. 16/17) (**Fig.S1B,C**). These data indicated that ISCs (*foxi1*) were generated at low levels, MCCs (*foxj1*) at low to medium levels, SSCs (*foxa1*) at medium to high levels, and that BCs (*ΔN-tp63*) were promoted by NICD. Goblet cells were not analyzed, as they emerge earlier through asymmetric cell division(Huang and Niehrs, 2014).

Next, we analyzed transcriptional changes over time in control and manipulated *Xenopus* mucociliary organoids by mRNA-sequencing (RNA-seq). Based on both published(Haas et al., 2019; Quigley and Kintner, 2017) and our own data, we defined marker sets for each cell type including factors necessary and sufficient to induce cell fates (**Fig.S2A,B**). Expression dynamics of these markers confirmed that cell fate specification starts at st. 9/10 (shortly after mid-blastula transition, MBT(Jukam et al., 2017)) and is largely accomplished by st. 16 as early markers increase only between st. 9-16 (**Fig.S2A,B**).

RNA-seq at st. 10, 16, 25 and 32 after manipulations confirmed that Notch inhibition strongly induced ISCs, decreased MCC marker expression at st. 16, and suppressed SSCs as well as BCs (**Fig.1C; S2B**). Interestingly, MCC marker expression recovered during later stages, which might explain why MCC numbers are not reduced by Notch inhibition. Notch overactivation suppressed ISCs and MCCs, but promoted expression of SSC and BC markers (**Fig.1C; S2B**).

Contrary to the current assumption that ISCs and MCCs are specified both by the lack of Notch signaling, these data indicate that MCCs are specified at higher Notch levels than ISCs, but at lower levels than SSCs and BCs.

162 **Cell types are specified sequentially by a temporal Notch signaling gradient**

163 We plotted RNA-seq expression levels (normalized to TPM) of cell type master
164 regulators over developmental time. This showed that *foxi1* (ISCs) was expressed first
165 and peaked by st. 12, while *gmnc* and *mcidas* (MCCs) were expressed from st. 10/11
166 and *mcidas* peaked at st. 16 (**Fig.1D**). *foxa1* and *spdef* (SSCs) expression started at
167 st. 11/12 and either peaked at st. 16 (*spdef*) or further increased until st. 32 (*foxa1*),
168 while *ΔN-tp63* (BCs) expression started at st. 16 and peaked at st. 25 (**Fig.1D**). These
169 results were confirmed by WMISH (**Fig.S2C,D**) and revealed the sequential initiation
170 of cell type specification in the *Xenopus* epidermis.

171 These results predicted a systemic increase in Notch signaling during specification.
172 Using quantitative RT-PCR (qPCR) on mucociliary organoids injected with a Notch
173 reporter (*4xcsl::H2B-mvenus*)(Nowotschin et al., 2013), we detected an increase in
174 signaling at st. 9-12, sustained activity until st. 16, and decrease in activity until st. 25
175 (**Fig.1E**).

176 Delta-like 1 (Dll1) was previously implicated in mucociliary patterning(Deblandre et al.,
177 1999), but other Notch components were not systematically analyzed so far. We found
178 that *dll1* and *notch1* were the increasingly and dominantly expressed ligand and
179 receptor, respectively (**Fig.1F and S3A**). RNA-seq and WMISH revealed that *notch1*
180 increased until st. 11 and was homogenously expressed in the basal layer of the
181 epidermis, while *dll1* expression increased for a longer time and was expressed by
182 differentiating cells (starting to undergo intercalation;(Deblandre et al., 1999)) (**Fig.1F;**
183 **S3B,C**).

184 To validate that graded Dll1 levels could tune cell type composition, we knocked down
185 *dll1* by different (low to high) morpholino-oligonucleotide (MO) concentrations.
186 Analysis of cell type markers at st. 16/17 confirmed that modifying Dll1 levels sufficed
187 to coordinately shift cell type ratios (**Fig.1G,H**). Thus, the initiation of and temporal
188 increase in ligand expression were critical parameters for patterning the mucociliary
189 system.

190 Loss-of-function experiments targeting all ligands and receptors (except for *dll4*)
191 followed by WMISH at st. 16/17 revealed that the depletion of any ligand or receptor
192 affected mucociliary patterning but to variable degrees (**Fig.S4**). Especially SSCs that
193 are specified last, were robustly reduced after knockdown of ligands and receptors
194 (**Fig.S4**). Thus, the sum of all ligands and receptors generates Notch levels required
195 for a correct cell type composition, similar to findings in the mammalian airway
196 epithelium(Morimoto et al., 2012).

197 In conclusion, we found that mucociliary cell types specification is initiated
198 sequentially, from low Notch-dependent ISCs to high Notch-dependent BCs. The
199 increase in signaling is predominantly achieved by ligand expression from a growing
200 pool of differentiating cells.

201 **Foxi1 induces ligand-expressing multipotent progenitors**

202 Similar expression dynamics (**Fig.1D,F**) and previous reports suggested a role for
203 Foxi1 in *dll1* regulation(Quigley and Kintner, 2017). Analysis of ligand and receptor

204 expression after Notch manipulations as well as after depletion of MCCs, SSCs or BCs
205 confirmed that blocking specification by NICD suppressed *dll1* and *dlc.L* ligands, and
206 revealed the induction of *notch* receptors (**Fig.S5A**)(Dubaissi et al., 2014; Haas et al.,
207 2019; Quigley and Kintner, 2017). In all other conditions, where *foxi1* expression was
208 stimulated, *dll1* and *dlc.L* were increased (**Fig.S5A**).

209 We overexpressed *foxi1*, *mcidas*, *foxj1*, *foxa1* or *ΔN-tp63*, and analyzed *dll1* and *dlc*
210 induction before the onset of their endogenous expression. Only *foxi1* robustly induced
211 *dll1/dlc* (**Fig.2A; S5B,C**). To test whether *foxi1* was acting directly, we analyzed
212 induction at MBT (st. 8) and additionally, at the onset of any transcription (st.6/7), which
213 showed *dll1/dlc* induction at both stages (**Fig.2B; S5D,E**). Conversely, depletion of
214 Foxi1 prevented *dll1* expression and caused embryonic lethality (**Fig.S5F-H**), in line
215 with previous reports(Mir et al., 2007).

216 Foxi1 could have an additional role during mucociliary development besides ISC
217 specification(Mir et al., 2007; Yan et al., 2006). We overexpressed *foxi1* and analyzed
218 mucociliary markers at st. 6/7. We found strong induction of *mcidas* (MCCs) as well
219 as weaker induction of *foxa1* (SSCs) and *ΔN-tp63* (BCs) by Foxi1 (**Fig.2C; S5I**). This
220 supported a novel role for Foxi1 in the induction of multipotent mucociliary progenitors.

221 In summary, the onset of *foxi1* expression induces mucociliary development and
222 multipotent mucociliary progenitors, which predominantly express *dll1/dlc* ligands to
223 increase Notch signaling during cell fate specification.

224

225 **Foxi1 and Notch regulate sequential Hes transcription factor expression**

226 Notch signaling confers cell fate decisions through Hairy enhancer of split (Hes/Hey)
227 transcription factors. Multiple Hes proteins have been implicated in mucociliary
228 patterning across models, but how they are employed for cell fate decisions remains
229 unresolved(Gomi et al., 2015; Morimoto et al., 2010; Ou-Yang et al., 2013; Tsao et al.,
230 2008; Tsao et al., 2009).

231 We analyzed how all known *Xenopus hes*/*hey* genes react to Notch manipulations,
232 and investigated their temporal expression dynamics in mucociliary organoids by
233 RNA-seq (**Fig.S6A,B**). We found that *hes7* paralogs were expressed first, followed by
234 *hes4* paralogs, and *hes1/hes5* paralogs (**Fig.S6B**). Within the four paralog groups,
235 *hes7.1.L (hes7.1)*, *hes4.L/.S (hes4)*, *hes5.10.L/.S (hes5.10)*, and *hes1.L/.S (hes1)*
236 were the dominantly expressed members.

237 *hes7.1* and *hes1* were inhibited by NICD, due to auto-(Kageyama et al., 2007) or Notch
238 repression(Takada et al., 2005), while *hes4* and *hes5.10* were induced by NICD, with
239 *hes5.10* showing a stronger response (**Fig.2D; S6A**). We confirmed the expression of
240 these *hes* genes by WMISH and found that *hes7.1* was expressed only in the deep
241 cell layer; *hes4* and *hes5.10* were expressed across both cell layers with variable
242 expression levels between individual cells; and *hes1* was expressed weakly and only
243 in a few cells (**Fig.2E; S6C,D**).

244 These data indicate that *hes7.1* is expressed in early progenitors and turned off by
245 increased Notch, suggesting a potential role in the initiation of mucociliary patterning.

Brislinger et al. Figure 2

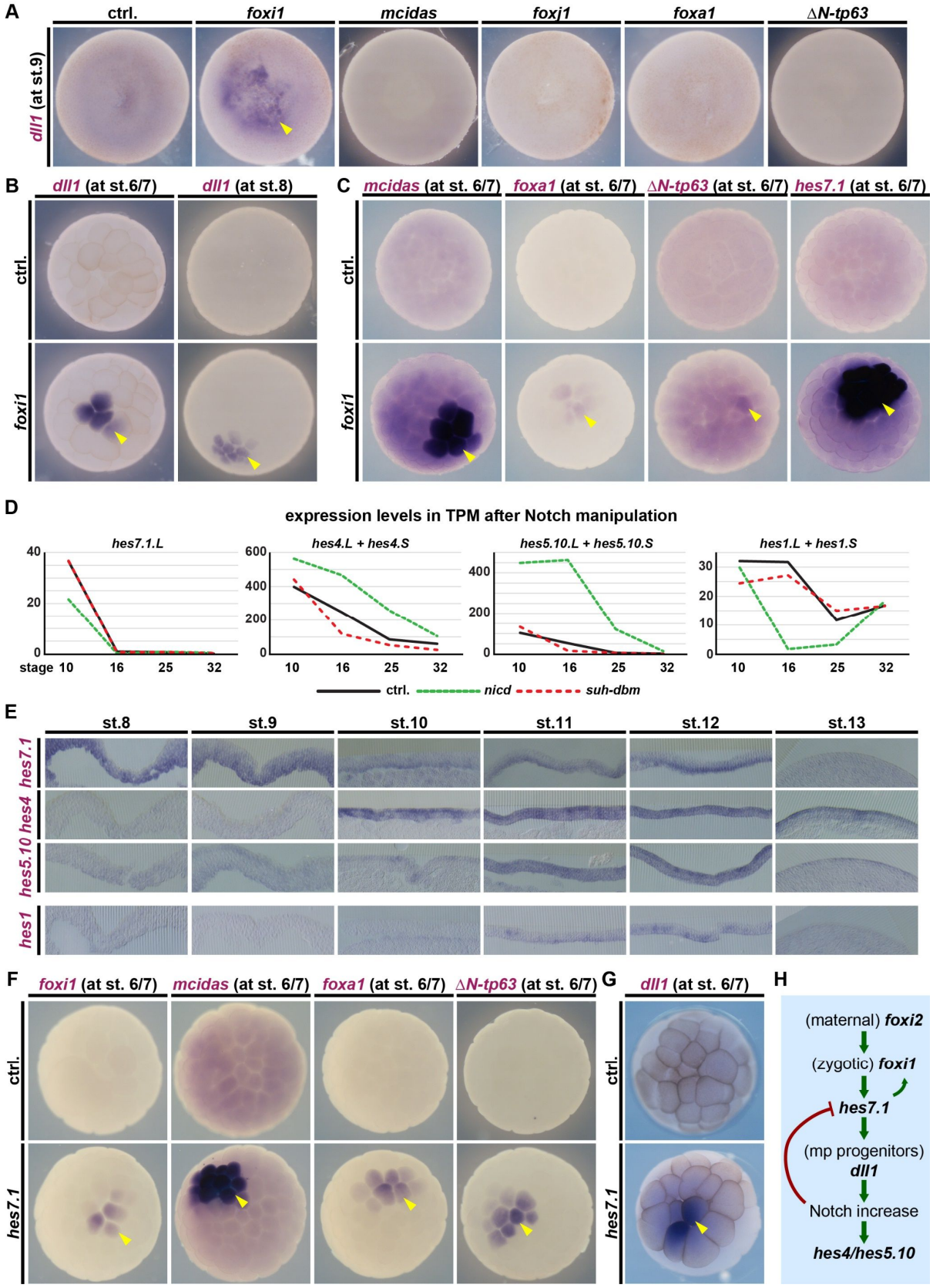

Figure 2: Foxi1 induces multipotent ligand-expressing progenitors via *hes7.1*

A-C, F,G: Animal view, WMISH. **A:** *dll1* at st. 9 in controls and after overexpression of master cell type inducers. Only *foxi1* induces *dll1* expression (yellow arrowhead). **B:** *dll1* at st. 6/7 and 8 in controls and

after *foxi1* (induction=yellow arrowhead). **C:** Marker gene expression at st. 6/7 in controls and after *foxi1* (induction=yellow arrowhead). **D:** Expression levels of indicated *hes* transcripts in unmanipulated mucociliary organoids (black line) and after Notch manipulations (loss=red line; gain=green line) across different stages of development (RNA-seq). **E:** Epidermis sections, WMISH for indicated *hes* transcripts from st. 8 to st. 13. **F,G:** Marker gene expression at st. 6/7 in controls and after *hes7.1* (induction=yellow arrowhead). **H:** Schematic summary of Notch, *hes* and *dll1* regulation in multipotent progenitors.

We overexpressed *hes7.1* and analyzed cell type marker induction. *hes7.1* was able to induce all markers as well as *dll1* at st. 6/7 (**Fig.2F,G; 3A; S7A**), similar to Foxi1. Overexpression of *foxi1* induced *hes7.1* expression at st. 6/7, while *foxi1*MO inhibited *hes7.1* expression at st. 9 (**Fig.2C; S7B-D**).

Taken together, we identified a set of sequentially expressed and Notch-regulated Hes transcription factors, and found that Foxi1 establishes multipotent mucociliary progenitors, at least in part, by initializing *hes7.1.L* expression (**Fig.2H**).

Hes factors act in a cell type-specific and concentration-dependent manner

hes4 seems to be induced by intermediate and *hes5.10* by high Notch levels, which suggests that they could integrate signaling levels during patterning. Interestingly, *hes1* expression and its reaction to Notch manipulations argued against a prominent role in cell fate specification in *Xenopus*, similar to findings from the mouse airways(Tsao et al., 2009).

In induction assays, *hes4* only induced MCC fate while *hes5.10* induced MCC, SSC and BC fates (**Fig.3A-C; S7E**). Graded responses were observed for the induction of MCCs by Hes4, which was more efficient at higher levels, and for BC induction by Hes5.10, which was more efficient at lower levels (**Fig.3A-C; S7E**). These results argued for cell type-specificity of *hes* genes during mucociliary patterning.

To reveal the endogenous effects of these Hes factors, we conducted loss-of-function experiments using low and high MO concentrations, and analyzed marker expression at st. 16/17. Mild (+) and strong (++) knockdown of all Hes factors suppressed SSCs and promoted ISC specification, with *hes4*MO having the strongest effect (**Fig.3D-G; S7F-H**). MCC specification was promoted (*hes7.1*MO and *hes5.10*MO) or remained unaffected (*hes4*MO) after mild knockdown, but was reduced by strong knockdowns of the tested Hes factors (**Fig.3D-G; S7F-H**). BCs were relatively unaffected by Hes knockdown (**Fig.3D-G; S7F-H**), suggesting the presence of an additional Notch-dependent factor regulating *ΔN-tp63*.

Thus, we have identified a set of differentially Notch-regulated *hes* paralogs with sequential expression, which regulate sequential cell fate specification. *hes7.1* is first expressed, restricted to progenitors and negatively Notch-regulated. *hes4* is activated next at intermediate Notch levels, suppressing ISCs while predominantly promoting MCCs. *hes5.10* is activated last by high Notch signaling and required for SSC specification. The overall weak effects of Hes depletions on BCs indicate additional Hes-independent routes of Notch-dependent *ΔN-tp63* regulation.

Brislinger et al. Figure 3

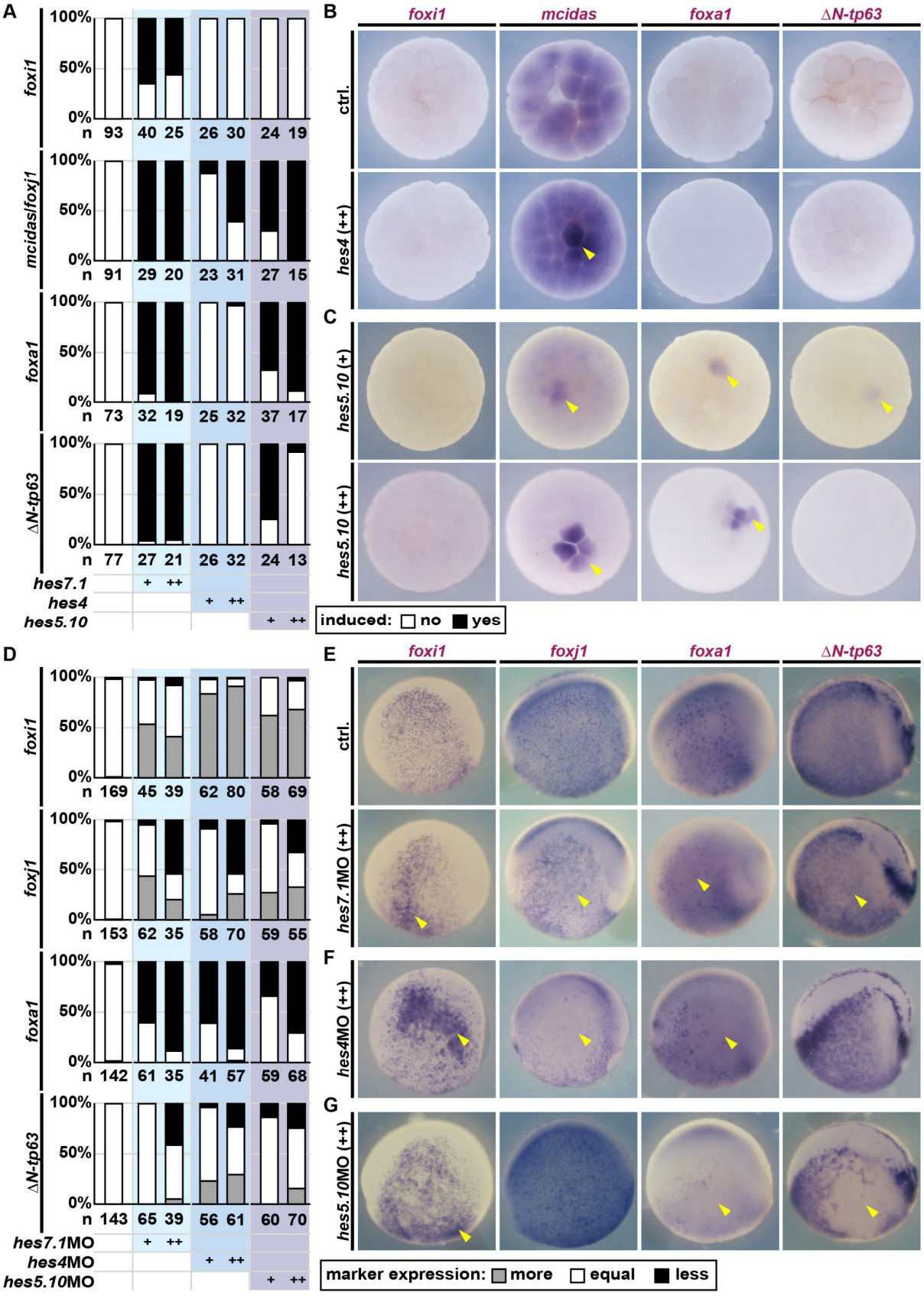

Figure 3: Hes factors regulate mucociliary cell fates

A: Quantification of results depicted in B,C. **B,C:** Animal view, WMISH. Marker gene expression at st. 6/7 in controls and after overexpression of indicated *hes*, +=low dose; ++=high dose (induction=yellow arrowhead). **D:** Quantification of results depicted in E-G. Expression levels were scored more, equal, less expression on the injected vs. uninjected side. **E-G:** Lateral view, WMISH. Marker gene expression at st. 16/17 in controls and after knockdown of indicated *hes*, +=low dose; ++=high dose (changes in expression=yellow arrowhead).

Hes factors act through competitive de-repression of cell fate choices

The *Xenopus* embryo is largely transcriptionally silent before MBT, in part because of the presence of repressors(Schulz and Harrison, 2019; Skirkanich et al., 2011). Hes factors are repressors, supporting the hypothesis that *hes7.1* could induced mucociliary genes by competitive de-repression of a maternally deposited stronger inhibitor(Jukam et al., 2017; Kageyama et al., 2007). Another Hes family member could potentially restrict mucociliary genes pre-MBT(Kageyama et al., 2007).

Using xenbase.org(Karpinka et al., 2014), we identified *hes2.L* as the most abundant maternal deposited *hes* (**Fig.4A**). We knocked down *hes2* by MO injections, which robustly induced premature *foxi1* at st. 9, while *mcidas* induction was hard to assess, and *foxa1*/*ΔN-tp63* were not induced (**Fig.4B; S8A**). Analysis of mucociliary transcripts by qPCR at st. 7/8 confirmed de-repression of *foxi1* and *mcidas* by *hes2*MO, and less robust elevation of *foxa1* and *ΔN-tp63* (**Fig.4C**). Conversly, overexpression of *hes2* disrupted expression of *foxi1* and *mcidas* at st. 12 (**Fig.4C; S8B,C**) as revealed by WMISH.

These results suggest that Hes2 acts as strong maternal repressor of mucociliary genes, and that the weak repressor Hes7.1 de-represses mucociliary gene activity at MBT. Subsequently, Hes4 and Hes5.10 are expressed in a Notch-dependent manner to promote MCC and SSC/BC fates by selective repression of alternative cell fates (**Fig.4E**).

A mathematical model emulates mucociliary patterning *in silico*

To test our understanding of the newly defined self-organizing mechanism (**Fig.S8D,E**), we used our experimentally-based hypotheses for building a minimal-component mathematical model of the generation of mucociliary cell type ratios (see methods for modeling details), and Principal Coordinate Analysis (PCoA) to fine-stage RNA-seq data (**Fig.S9A-C; Table S1**). Maximum likelihood estimates of the parameter values were derived by fitting data from time-resolved RNA-seq and cell type quantifications (**Fig.4F; S10A-D**). Using this approach, we found a solution (model 1) that recapitulated the endogenous generation of cell type composition, but which failed to fit dynamic ligand levels as well as *hes5* expression (**Fig.S10A,G**), and which failed to predict cell type production phases for Notch gain- and loss-of-function experiments (**Fig.S10E,F**). Furthermore, prediction of the effect of altering the production rate of ligands from multipotent progenitors contradicted experimental results (**Fig.S10H**; cf. **Fig.1A,G,H**). This indicated, that missing knowledge on how *ΔN-tp63* and BCs are maintained even when Notch levels decrease constituted a major gap in the model.

Brislinger et al. Figure 4

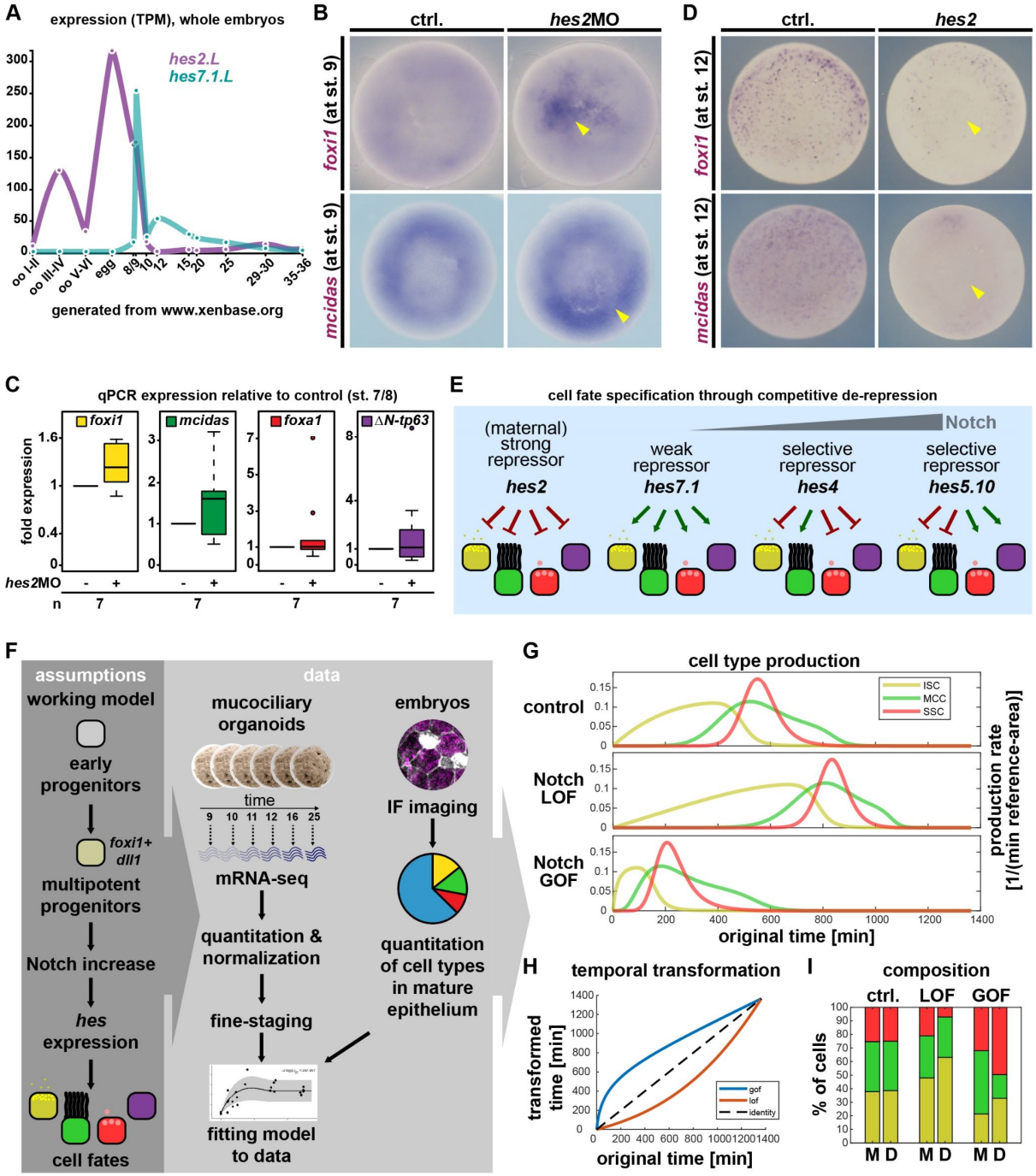

Figure 4: Competitive de-repression and modeling of mucociliary cell fate decisions
A: Expression levels of *hes2.L* and *hes7.1.L* in whole *Xenopus* eggs and embryos during early development. (RNA-seq.) **B:** Animal view, WMISH. Marker gene expression at st. 9 in controls and after knockdown of *hes2*. (induction=yellow arrowhead). **C:** Induction of mucociliary marker genes after knockdown of hes2 at st. 7/8 in whole embryos. (qPCR). **D:** Ventral view, WMISH. Marker gene expression at st. 12 in controls and after overexpression of *hes2*. (loss of expression=yellow arrowhead). **E:** Schematic summary of Hes-mediated competitive de-repression of cell fates in *Xenopus*. **F:** Schematic representation of minimal-component model building. **G-I:** *In silico* modeling of the cell fate specification process. **G:** Cell type production rates over time (control), and the effect of deceleration (LOF) or acceleration (GOF) on the production rates of ISCs, MCCs, and SSCs. **H:** The *in-silico* model could explain Notch loss- (LOF) and gain-of-function (GOF) experiments by deceleration (LOF) or acceleration (GOF) of the whole cell specification process via the depicted nonlinear

transformation of the time axis. **I:** Comparison of modeled [M] and experimentally determined [D] cell type ration of ISCs (yellow), MCCs (green) and SSCs (red).

The Ets-transcription factor Spdef is Notch-regulated and required for secretory cells in the mammalian airways(Guseh et al., 2009; Rock et al., 2011), but it is also expressed in human airway basal cells (https://www.proteinatlas.org/ENSG00000124664-SPDEF/summary/rna)(Karlsson et al., 2021). In *Xenopus* mucociliary organoids, *spdef* expression precedes SSC specification and the initiation of *ΔN-tp63* (**Fig.1D**). We therefore speculated that Spdef could promote SSC-specification at lower levels, while blocking SSCs and promoting BC at higher levels. Thereby, it could provide a switch for the transition from specification to long-term maintenance of mucociliary patterns, and allowing for the drop in Notch ligand expression after st. 16 (**Fig.1E,F**). We introduced these regulatory connections into our mathematical model, re-fitted parameters, and modeled cell type production (model 2) (**Fig.4G; S9C**). Model 2 improved fitting quality (**Table S2**), and could explain Notch gain- and loss-of-function effects by a temporal transformation representing de- (for LOF) and acceleration (for GOF) of cell type production rates (**Fig.4G-I; S10B,D**). Furthermore, model 2 also generated results in line with experimental observations on altering ligand expression from multipotent progenitors (**Fig.S10I**; cf. **Fig.1A,G,H**).

Taken together, we were able to generate a minimal component mathematical model that recapitulates normal mucociliary patterning *in silico*, and that can be used to predict critical gaps in our understanding of mucociliary patterning - in our case, modeling predicts an additional role for Spdef in Notch-mediated regulation of BCs.

Discussion:

We elucidated how a morphogen-like temporal Notch gradient regulates mucociliary cell type composition in *Xenopus*. We found a novel role for Foxi1 in the induction of *hes7.1* to generate Notch ligand-expressing multipotent progenitors, which partially explains why it acts as ectodermal determinant(Mir et al., 2007). Expansion of the progenitor population increases systemic Notch levels, inhibiting *hes7.1* and inducing first *hes4*, then *hes5.10* to specify other cell types. This self-organized patterning system leads to sequential initiation of cell type specification, and the generation of correct cell numbers and ratios. Our data indicate that a set of repressors is used to regulate onset of mucociliary development as well as cell fate decisions. This suggests that cell fates are not actively induced, but facilitated by restricting alternative fate choices in multipotent progenitors. Thus, we refer to this mode of regulation as “competitive de-repression”.

foxi1 is induced by maternally deposited Foxi2 at MBT(Cha et al., 2012) and is negatively regulated by Hes4/Hes5.10. Sustained Foxi1 specifies ISC fate, and consequently, ISCs are specified first and only at very low Notch levels. *hes4* is induced at intermediate Notch levels and favors MCC specification, while *hes5.10* is induced at higher Notch levels and required for SSCs, which are specified last. BC are

promoted by Notch and partially by Hes5.10, but our results suggest additional Hes-independent routes of *ΔN-tp63* regulation, which need further investigation. Our minimal-component *in silico* model recapitulates some of the most important features of the patterning process, such as the order of cell fate specification, temporal dependency, and changes in cell type compositions upon reduced Notch ligand expression. It the latter case, it produces results in line with our own and published data, e.g. the over-production of MCCs after Notch loss-of-function, that cannot be fully appreciated in our IF datasets, because not all MCCs can intercalate into the outer epithelium(Stubbs et al., 2006). Furthermore, the model predicts a new function of Spdef, which can be tested in future experiments.

In the mammalian lung, developmental time and location are coupled, with new cells emerging at the growing distal tips(Morimoto et al., 2010; Tsao et al., 2008). ISCs are rare and specified by higher Notch levels indicating that Foxi1 is not required for lung mucociliary development(Montoro et al., 2018). MCCs are specified first, emerge more distally than club cells, and produce Jag1/Jag2 ligands required for club cell specification(Morimoto et al., 2010; Rawlins et al., 2007), indicating a conservation of the general patterning mechanism. Airway BCs are not positively regulated by Notch during patterning, but sustained Notch inhibition prevents differentiation of MCCs and secretory cells in human ALI cultures, and leads to the thinning of the epithelium(Gomi et al., 2015; Rock et al., 2011), strongly suggesting a positive role for Notch in mammalian BCs maintenance as well. Similar to *Xenopus*, Hes5 is required for secretory cells, while Hes1 does not play a dominant role in mucociliary patterning in mammals(Tsao et al., 2009; Xing et al., 2012). Whether a similar competitive de-repression mechanism exists in airway mucociliary development remains unclear, but recent reports suggest a potentially similar function to Hes7.1 for Inhibitor of differentiation 2 (Id2) in the regulation of basal cells and differentiation(Kiyokawa et al., 2021).

Hence, we have uncovered a novel and potentially highly conserved self-organization mechanism regulating mucociliary cell type composition in vertebrates.

References:

Briggs, J. A., Weinreb, C., Wagner, D. E., Megason, S., Peshkin, L., Kirschner, M. W. and Klein, A. M. (2018). The dynamics of gene expression in vertebrate embryogenesis at single-cell resolution. *Science (80-.).* **360**, eaar5780.

Cha, S. W., McAdams, M., Kormish, J., Wylie, C. and Kofron, M. (2012). Foxi2 is an animally localized maternal mRNA in xenopus, and an activator of the zygotic ectoderm activator foxi1e. *PLoS One* **7**, 1–10.

Community, T. G. (2022). The Galaxy platform for accessible , reproducible and collaborative biomedical analyses : 2022 update. *Nucleic Acids Res.* **50**, 345–351.

Deblandre, G. A., Wettstein, D. A., Koyano-Nakagawa, N. and Kintner, C. (1999). A two-step mechanism generates the spacing pattern of the ciliated cells in the skin of Xenopus embryos. *Development* **126**, 4715–4728.

Dobin, A., Davis, C. A., Schlesinger, F., Drenkow, J., Zaleski, C., Jha, S., Batut, P., Chaisson, M. and Gingeras, T. R. (2013). STAR: ultrafast universal RNA-seq aligner. *Bioinformatics* **29**, 15–21.

436 **Dubaissi, E., Rousseau, K., Lea, R., Soto, X., Nardeosingh, S., Schweickert, A., Amaya, E.,**
437 **Thornton, D. J. and Papalopulu, N.** (2014). A secretory cell type develops alongside
438 multiciliated cells, ionocytes and goblet cells, and provides a protective, anti-infective function in
439 the frog embryonic mucociliary epidermis. *Development* **141**, 1514–25.

440 **Fortriede, J. D., Pells, T. J., Chu, S., Chaturvedi, P., Wang, D., Fisher, M. E., James-zorn, C.,**
441 **Wang, Y., Nenni, M. J., Burns, K. A., et al.** (2020). Xenbase : deep integration of GEO & SRA
442 RNA-seq and ChIP-seq data in a model organism database. *Nucleic Acids Res.* **48**, 776–782.

443 **Gomi, K., Arbelaez, V., Crystal, R. G. and Walters, M. S.** (2015). Activation of NOTCH1 or NOTCH3
444 Signaling Skews Human Airway Basal Cell Differentiation toward a Secretory Pathway. *PLoS*
445 *One* **10**, e0116507.

446 **Guseh, J. S., Bores, S. A., Stanger, B. Z., Zhou, Q., Anderson, W. J., Melton, D. A. and**
447 **Rajagopal, J.** (2009). Notch signaling promotes airway mucous metaplasia and inhibits alveolar
448 development. *Development* **136**, 1751–1759.

449 **Haas, M., Gómez Vázquez, J. L., Sun, D. I., Tran, H. T., Brislinger, M., Tasca, A., Shomroni, O.,**
450 **Vleminckx, K. and Walentek, P.** (2019). ΔN-Tp63 Mediates Wnt/β-Catenin-Induced Inhibition
451 of Differentiation in Basal Stem Cells of Mucociliary Epithelia. *Cell Rep.* **28**, 3338-3352.e6.

452 **Harland, R. M. and Biology, C.** (1991). In situ hybridization: an improved whole-mount method for
453 Xenopus embryos. *Methods Cell Biol.* **36**, 685–95.

454 **Hayes, J. M., Kim, K. S., Abitua, P. B., Park, T. J., Herrington, E. R., Kitayama, A., Grow, M. W.,**
455 **Ueno, N. and Wallingford, J. B.** (2007). Identification of novel ciliogenesis factors using a new
456 in vivo model for mucociliary epithelial development. *Dev. Biol.* **312**, 115–30.

457 **Hogan, B. L. M., Barkauskas, C. E., Chapman, H. A., Epstein, J. A., Jain, R., Hsia, C. C. W.,**
458 **Niklason, L., Calle, E., Le, A., Randell, S. H., et al.** (2014). Repair and Regeneration of the
459 Respiratory System: Complexity, Plasticity, and Mechanisms of Lung Stem Cell Function. *Cell*
460 *Stem Cell* **15**, 123–138.

461 **Huang, Y. and Niehrs, C.** (2014). Polarized Wnt signaling regulates ectodermal cell fate in Xenopus.
462 *Dev. Cell* **29**, 250–7.

463 **Jukam, D., Shariati, S. A. M. and Skotheim, J. M.** (2017). Zygotic Genome Activation in
464 Vertebrates. *Dev. Cell* **42**, 316–332.

465 **Kageyama, R., Ohtsuka, T. and Kobayashi, T.** (2007). The Hes gene family: Repressors and
466 oscillators that orchestrate embryogenesis. *Development* **134**, 1243–1251.

467 **Karlsson, M., Zhang, C., Méar, L., Zhong, W., Digre, A., Katona, B., Sjöstedt, E., Butler, L.,**
468 **Odeberg, J., Dusart, P., et al.** (2021). A single–cell type transcriptomics map of human tissues.
469 *Sci. Adv.* **7**, 1–10.

470 **Karpinka, J. B., Fortriede, J. D., Burns, K. a, James-Zorn, C., Ponferrada, V. G., Lee, J., Karimi,**
471 **K., Zorn, A. M. and Vize, P. D.** (2014). Xenbase, the Xenopus model organism database; new
472 virtualized system, data types and genomes. *Nucleic Acids Res.* **43**, 756–763.

473 **Kiyokawa, H. and Morimoto, M.** (2020). Notch signaling in the mammalian respiratory system,
474 specifically the trachea and lungs, in development, homeostasis, regeneration, and disease.
475 *Dev. Growth Differ.* **62**, 67–79.

476 **Kiyokawa, H., Yamaoka, A., Matsuoka, C., Tokuhara, T., Abe, T. and Morimoto, M.** (2021). Airway
477 basal stem cells reutilize the embryonic proliferation regulator, Tgfβ-Id2 axis, for tissue
478 regeneration. *Dev. Cell* **56**, 1917-1929.e9.

479 **Liao, Y., Smyth, G. K. and Shi, W.** (2014). featureCounts: an efficient general purpose program for
480 assigning sequence reads to genomic features. *Bioinformatics* **30**, 923–930.

481 **Love, M. I., Huber, W. and Anders, S.** (2014). Moderated estimation of fold change and dispersion
482 for RNA-seq data with DESeq2. *Genome Biol.* **15**, 1–21.

483 **Mir, A., Kofron, M., Zorn, A. M., Bajzer, M., Haque, M., Heasman, J. and Wylie, C. C.** (2007).

484 FoxI1e activates ectoderm formation and controls cell position in the Xenopus blastula.
485 *Development* **134**, 779–88.

486 **Montoro, D. T., Haber, A. L., Biton, M., Vinarsky, V., Lin, B., Birket, S. E., Yuan, F., Chen, S.,**
487 **Leung, H. M., Villoria, J., et al.** (2018). A revised airway epithelial hierarchy includes CFTR-
488 expressing ionocytes. *Nature* **560**, 319–324.

489 **Morimoto, M., Liu, Z., Cheng, H.-T., Winters, N., Bader, D. and Kopan, R.** (2010). Canonical Notch
490 signaling in the developing lung is required for determination of arterial smooth muscle cells and
491 selection of Clara versus ciliated cell fate. *J. Cell Sci.* **123**, 213–24.

492 **Morimoto, M., Nishinakamura, R., Saga, Y. and Kopan, R.** (2012). Different assemblies of Notch
493 receptors coordinate the distribution of the major bronchial Clara, ciliated and neuroendocrine
494 cells. *Development* **139**, 4365–4373.

495 **Nenni, M. J., Fisher, M. E., James-Zorn, C., Pells, T. J., Ponferrada, V., Chu, S., Fortriede, J. D.,**
496 **Burns, K. A., Wang, Y., Lotay, V. S., et al.** (2019). XenBase: Facilitating the use of Xenopus to
497 model human disease. *Front. Physiol.* **10**, 1–13.

498 **Nowotschin, S., Xenopoulos, P., Schrode, N. and Hadjantonakis, A. K.** (2013). A bright single-cell
499 resolution live imaging reporter of Notch signaling in the mouse. *BMC Dev. Biol.* **13**, 1.

500 **Ou-Yang, H. F., Wu, C. G., Qu, S. Y. and Li, Z. K.** (2013). Notch signaling downregulates MUC5AC
501 expression in airway epithelial cells through hes1-dependent mechanisms. *Respiration* **86**, 341–
502 346.

503 **Quigley, I. K. and Kintner, C.** (2017). Rfx2 Stabilizes Foxj1 Binding at Chromatin Loops to Enable
504 Multiciliated Cell Gene Expression. *PLoS Genet.* 1–29.

505 **Quigley, I. K., Stubbs, J. L. and Kintner, C.** (2011). Specification of ion transport cells in the
506 Xenopus larval skin. *Development* **138**, 705–714.

507 **Raue, A., Steiert, B., Schelker, M., Kreutz, C., Maiwald, T., Hass, H., Vanlier, J., Tönsing, C.,**
508 **Adlung, L., Engesser, R., et al.** (2015). Data2Dynamics: A modeling environment tailored to
509 parameter estimation in dynamical systems. *Bioinformatics* **31**, 3558–3560.

510 **Rawlins, E. L., Ostrowski, L. E., Randell, S. H. and Hogan, B. L. M.** (2007). Lung development and
511 repair: Contribution of the ciliated lineage. *Proc. Natl. Acad. Sci. U. S. A.* **104**, 410–417.

512 **Rock, J. R., Gao, X., Xue, Y., Randell, S. H., Kong, Y. Y. and Hogan, B. L. M. M.** (2011). Notch-
513 dependent differentiation of adult airway basal stem cells. *Cell Stem Cell* **8**, 639–648.

514 **Schindelin, J., Arganda-Carreras, I., Frise, E., Kaynig, V., Longair, M., Pietzsch, T., Preibisch,**
515 **S., Rueden, C., Saalfeld, S., Schmid, B., et al.** (2012). Fiji: an open-source platform for
516 biological-image analysis. *Nat. Methods* **9**, 676–82.

517 **Schulz, K. N. and Harrison, M. M.** (2019). Mechanisms regulating zygotic genome activation. *Nat.*
518 *Rev. Genet.* **20**, 221–234.

519 **Session, A. M., Uno, Y., Kwon, T., Chapman, J. A., Toyoda, A., Takahashi, S., Fukui, A.,**
520 **Hikosaka, A., Suzuki, A., Kondo, M., et al.** (2016). Genome evolution in the allotetraploid frog
521 Xenopus laevis. *Nature* **538**, 336–343.

522 **Sive, H. L., Grainger, R. M. and Harland, R. M.** (2000). *Early Development of Xenopus laevis*. Cold
523 Spring Harbor, NY, USA: Cold Spring Harbor Laboratory Press.

524 **Sive, H. L., Grainger, R. M. and Harland, R. M.** (2010). Microinjection of xenopus oocytes. *Cold*
525 *Spring Harb. Protoc.* **5**,.

526 **Skirkanich, J., Luxardi, G., Yang, J., Kodjabachian, L. and Klein, P. S.** (2011). An essential role
527 for transcription before the MBT in Xenopus laevis. *Dev. Biol.*

528 **Stubbs, J. L., Davidson, L., Keller, R. and Kintner, C.** (2006). Radial intercalation of ciliated cells
529 during Xenopus skin development. *Development* **133**, 2507–15.

530 **Stubbs, J. L., Oishi, I., Izpisúa Belmonte, J. C. and Kintner, C.** (2008). The forkhead protein Foxj1

specifies node-like cilia in Xenopus and zebrafish embryos. *Nat. Genet.* **40**, 1454–60.

Stubbs, J. L., Vladar, E. K., Axelrod, J. D. and Kintner, C. (2012). Multicilin promotes centriole assembly and ciliogenesis during multiciliate cell differentiation. *Nat. Cell Biol.* **14**, 1–10.

Takada, H., Hattori, D., Kitayama, A., Ueno, N. and Taira, M. (2005). Identification of target genes for the Xenopus Hes-related protein XHR1, a prepattern factor specifying the midbrain-hindbrain boundary. *Dev. Biol.* **283**, 253–267.

Tasca, A., Helmstädter, M., Brislinger, M. M., Haas, M., Mitchell, B. and Walentek, P. (2021). Notch signaling induces either apoptosis or cell fate change in multiciliated cells during mucociliary tissue remodeling. *Dev. Cell* **56**, 525-539.e6.

Tsao, P. N., Chen, F., Izvolsky, K. I., Walker, J., Kukuruzinska, M. A., Lu, J. and Cardoso, W. V. (2008). γ-Secretase activation of notch signaling regulates the balance of proximal and distal fates in progenitor cells of the developing lung. *J. Biol. Chem.* **283**, 29532–29544.

Tsao, P.-N. N., Vasconcelos, M., Izvolsky, K. I., Qian, J., Lu, J. and Cardoso, W. V. (2009). Notch signaling controls the balance of ciliated and secretory cell fates in developing airways. *Development* **136**, 2297–307.

Volckaert, T. and De Langhe, S. (2014). Lung epithelial stem cells and their niches: Fgf10 takes center stage. *Fibrogenes. Tissue Repair* **7**, 1–15.

Walentek, P. (2018). Manipulating and Analyzing Cell Type Composition of the Xenopus Mucociliary Epidermis. In *Methods in Molecular Biology*, pp. 251–263.

Walentek, P. (2021a). Signaling Control of Mucociliary Epithelia: Stem Cells, Cell Fates, and the Plasticity of Cell Identity in Development and Disease. *Cells Tissues Organs*.

Walentek, P. (2021b). Xenopus epidermal and endodermal epithelia as models for mucociliary epithelial evolution, disease, and metaplasia. *Genesis* 1–17.

Walentek, P. and Quigley, I. K. I. K. (2017). What we can learn from a tadpole about ciliopathies and airway diseases: Using systems biology in Xenopus to study cilia and mucociliary epithelia. *Genesis* **55**, 1–12.

Walentek, P., Beyer, T., Thumberger, T., Schweickert, A. and Blum, M. (2012). ATP4a is required for Wnt-dependent Foxj1 expression and leftward flow in Xenopus left-right development. *Cell Rep.* **1**, 516–27.

Walentek, P., Bogusch, S., Thumberger, T., Vick, P., Dubaissi, E., Beyer, T., Blum, M. and Schweickert, A. (2014). A novel serotonin-secreting cell type regulates ciliary motility in the mucociliary epidermis of Xenopus tadpoles. *Dev.* **141**, 1526–1533.

Whitsett, J. A. (2018). Airway epithelial differentiation and mucociliary clearance. *Ann. Am. Thorac. Soc.* **15**, S143–S148.

Xing, Y., Li, A., Borok, Z., Li, C., Minoo, P., Medicine, C., Angeles, L., Xing, Y., Li, A., Borok, Z., et al. (2012). NOTCH1 Is Required for Regeneration of Clara Cells During Repair of Airway Injury. *Stem Cells* **30**, 946–955.

Yan, J., Xu, L., Crawford, G., Wang, Z. and Burgess, S. M. (2006). The Forkhead Transcription Factor FoxI1 Remains Bound to Condensed Mitotic Chromosomes and Stably Remodels Chromatin Structure. *Mol. Cell. Biol.* **26**, 155–168.

Acknowledgments:

We thank: S. Schefold, M. Hansen, C. Softley for expert technical help; W. Driever, G. Pyrowolakis, C. Kintner for discussions and/or critical reading; Xenbase, EXRC for Xenopus resources; Light Imaging Center Freiburg and Aqua Core Facility for microscope/animal resources; B. Grüning and the Freiburg Galaxy Team for the

bioinformatics platform and continuous support. This study was supported by the Deutsche Forschungsgemeinschaft (DFG) under the Emmy Noether Programme (grant WA3365/2-1) and by the NHLBI through a Pathway to Independence Award (K99HL127275) to PW; and under Germany's Excellence Strategy (CIBSS – EXC-2189 – Project ID 390939984) to PW and CK.

Author contribution:

MMBE, SB, MH, AT, PW: Xenopus experiments; MMBE, PW: experimental design, planning, analysis and interpretation of data; FL, CK: Mathematical modeling; PW: bioinformatics, study design and supervision, coordinating collaborative work, manuscript preparation with input from all authors.

Methods:

Animal models and data availability

Xenopus laevis

Wild-type Xenopus laevis were obtained from the European Xenopus Resource Centre (EXRC) at University of Portsmouth, School of Biological Sciences, UK, or Xenopus 1, USA. Frog maintenance and care was conducted according to standard procedures in the AquaCore facility, University Freiburg, Medical Center (RI_00544) and based on recommendations provided by the international Xenopus community resource centers NXR (RRID:SCR_013731) and EXRC as well as by Xenbase (http://www.xenbase.org/, RRID:SCR_003280)(Nenni et al., 2019).

Ethics statements on animal experiments

This work was done in compliance with German animal protection laws and was approved under Registrier-Nr. G-18/76 by the state of Baden-Württemberg.

Material, data and code availability

NGS datasets are available via NCBI GEO (cf. RNA-sequencing on *Xenopus* mucociliary organoids and bioinformatics analysis). Imaging and quantification data are available to the scientific community upon request to peter.walentek@medizin.uni-freiburg.de. Mathematical modeling details and code are available to the scientific community upon request to ckreutz@imbi.uni-freiburg.de.

Xenopus experiments

Manipulation of Xenopus Embryos, Constructs and In Situ Hybridization

X. laevis eggs were collected and in vitro-fertilized, then cultured and microinjected by standard procedures (Sive et al., 2010). Embryos were injected with Morpholino oligonucleotides (MOs, Gene Tools), mRNAs or plasmid DNA at two-cell or four-cell stage using a PicoSpritzer setup in 1/3x Modified Frog Ringer's solution (MR) with 2.5% Ficoll PM 400 (GE Healthcare, #17-0300-50), and were transferred after injection into 1/3x MR containing Gentamycin. Drop size was calibrated to about 7–8nL per injection.

622 Embryos injected with hormone-inducible constructs of (GFP-ΔN-tp63-GR(Haas et al.,
623 2019) and MCI-GR(Stubbs et al., 2012)) were treated with 10µM Dexamethasone
624 (Sigma-Aldrich/Merck #D4902) in ethanol from eight-cell stage until fixation. Ultrapure
625 Ethanol (NeoFroxx #LC-8657.3) was used as vehicle control.
626 Morpholino oligonucleotides (MOs) were obtained from Gene Tools targeting *dlc, dll1,*
627 *foxa1, foxi1, hes2, hes4, hes5.10, hes7.1, jag1, jag2, notch1, notch2, notch3, and ΔN-*
628 *tp63,* and used at doses as indicated below.
629
630 Morpholino Sequences

Name	**Sequence**	**Concentration Range**
foxi1MO	5'-GTGCTTGTGGATCAAATGCACTCAT-3'	3 pmol
hes4.LMO	5'-CAGGCATGTTCAGATGTTGTATCCG-3'	1-4 pmol
hes5.10.L/SMO	5'-TGCAGATTGGGAGCCATTCTTTATG-3'	1-4 pmol
hes7.1.LMO	5'-CTTCACTTGTTCCCTTCATGGTAAG-3'	1-4 pmol
notch1MO	5'-GCACAGCCAGCCCTATCCGATCCAT-3'	1-4 pmol
notch2.L/sMO	5'-CAAACACAGCCTGCACCCCCATC-3'	3 pmol
notch3.L/sMO	5'-CCCATGATGCTCTCCTCCCCC-3'	3 pmol
dll1.LMO	5'-CCCATGTTGTCTGATATGCGATTG-3'	1-4 pmol
dll1.sMO	5'-AGGCACTGCTGTCCCATGTTG-3'	1-4 pmol
dlc.LMO	5'-CAGTCTCCTGGCACTGACAAGGTG-3'	3 pmol
jag1.LMO	5'-CTCTCCTTGGGAAACGCATTGCTTC-3'	4 pmol
jag2.L/sMO	5'-TACTTATATCCAACATTGCTGGGAA-3'	4 pmol
foxa1MO	5'-ATGGCAAGTGCCCGAGAGAATCATT-3'	3 pmol
tp63MO	5'-GATACAACATCTTTGCAGTGAGGTT-3'	4 pmol
hes2.LMO	5'-GCTCCCAATGTAGCGCTCGCAGACT-3'	5-8 pmol

631
632 Full-length *hes1, hes4, hes5.10, hes7.1* and *hes2* constructs were cloned from
633 total reverse-transcribed cDNA into pCS107 for overexpression and/or pGEM-T Easy
634 (Promega #A137A) for anti-sense probes using primers listed below. All sequences
635 were verified by Sanger sequencing and linearized with Apa1 (New England BioLabs
636 #R0114S) to generate mRNAs (used at 25-150ng/µl). Anti-sense probe templates
637 were either linearized with Sac2 (New England BioLabs #R0157S) and synthesized
638 with SP6 RNA polymerase (Promega #P108G) or Sac1 (New England BioLabs
639 #r3156S) and synthesized with T7 (Promega #P207E)
640
641 mRNA encoding membrane-GFP was used in some experiments as lineage
642 tracers at 50ng/µL. All mRNAs were prepared using the Ambion mMessage Machine
643 kit using Sp6 (#AM1340) supplemented with RNAse Inhibitor (Promega #N251B).
644
645 Notch reporter 4xcsl::H2B-mvenus plasmid(Nowotschin et al., 2013) was injected
646 at 30ng/µl after purification using the PureYield Midiprep kit (Promega, #A2492).
647 For antisense *in situ* hybridization probes, *notch1, notch2, notch3, dlc*, and *jag2* fragments
648 were cloned from whole-embryo cDNAs derived from stages between 3 and 30 using primers
649 listed below (ISH-primers). All sequences were verified by Sanger sequencing. In addition, the
650 following, previously published probes were used: *foxi1*(Quigley et al., 2011) , *foxj1*(Stubbs et
651 al., 2008), *mcidas*(Stubbs et al., 2012), *foxa1*(Hayes et al., 2007) , *tp63*(Haas et al., 2019),
652 *dll1*(Deblandre et al., 1999) and *jag1*(Tasca et al., 2021).

653

654 Cloning Primer Sequences

Name	Sequence
ISH-notch1-F	CATTATCTCCCATCTGCTCC
ISH-notch1-R	CGTCTGGTTTATGTCGCTG
ISH-notch2-F	CAAATTCTCTTTCACCAGCAG
ISH-notch2-R	GTTTGAGATAACTGTCCATCGT
ISH-notch3-F	GCTTCTGGAGGAACACAACAC
ISH-notch3-R	GTAACATCATTGGGCACGCT
ISH-dlc-F	GAAGATTGATCGCTGTACC
ISH-dlc-R	AATTGGGACTTTCTGATTGG
BamH1-hes1-F	AAAGGATCCATGCCGGCTGATGTGATGGAG
hes1-Sal1-R	AAAGTCGACTTACCAGGGCCTCCAAACAG
BamH1-hes4-F	AAAGGATCCATGCCTGCAGATAGTATGGAG
hes4-Sal1-R	AAAGTCGACTCACCATGGTCGCCACACGG
BamH1-hes5.10-F	AAAGGATCCATGGCTCCAAATCTGCAGATG
hes5.10-Sal1-R	AAAGTCGACTTAAGGAGGAGAAAGAACCTG
BamH1-hes7.1-F	AAAGGATCCATGAAGGGAACAAGTGAAGTC
hes7.1-Sal1-R	AAAGTCGACTCATACCCAGGGTCTCCAGG
BamH1-hes2-F	AAAAGGATCCATGGCTCCCAATGTAGC
hes2-Sal1-R	AAAAGTCGACTCACCACGGCCTCCAG

655

656 Whole mount in situ hybridization

657 Embryos were fixed in MEMFA (100mM MOPS pH7.4, 2mM EGTA, 1mM MgSO4,
658 3.7% (v/v) Formaldehyde) overnight at 4°C and stored in 100% Ethanol at -20°C until
659 used. DNAs were purified using the PureYield Midiprep kit and were linearized before
660 in vitro synthesis of anti-sense RNA probes using T7 or Sp6 polymerase (Promega,
661 #P2077 and #P108G), RNAse inhibitor and dig-labeled rNTPs (Roche, #3359247910
662 and 11277057001). Embryos were in situ hybridized according to (Harland and
663 Biology, 1991), bleached (Sive et al., 2000) after staining with BM Purple (Roche
664 #11442074001) and imaged. Sections were made after embedding in gelatin-albumin
665 with Glutaraldehyde at 70μm as described in (Walentek et al., 2012).

666

667 Stage series and morphological evaluations

668 Embryos were staged according to Nieuwkoop and Faber (1994) Normal Table
669 of *Xenopus laevis* (Daudin). Garland Publishing Inc, New York ISBN 0-8153-1896-0.
670 Onset of marker gene expression was quantified after *in situ* hybridization according
671 to the number of stained dots visible in (prospective) epidermal cells. Marker
672 expression was categorized into three groups (no expression; <20 dots; >20 dots).
673 For embryos injected with *foxi1*MO, cell morphology and cell size were evaluated to
674 determine that the embryos were dying. These embryos showed the features of
675 aberrant cell morphology, increased cell size and cells/whole embryos that had
676 completely turned white.

677

678 Preparation of mucociliary organoids (animal caps)

679 Injected and wildtype embryos were cultured until st. 8. Animal caps were dissected
680 in 1x Modified Barth's solution (MBS) and transferred to 0.5x MBS + Gentamycin(Sive
681 et al., 2000). 10-15 organoids were collected in TRIzol (Thermo Fisher #15596026)
682 per stage and used for qPCR or RNAsequencing.

683

684 Quantitative RT-PCR

685 Total RNA was extracted using a standard Trizol (Invitrogen #15596026) protocol
686 and used for cDNA synthesis with either iScript cDNA Synthesis Kit (Bio-Rad
687 #1708891) or for the Notch reporter analysis with iScript gDNA Clear cDNA Synthesis
688 Kit (Bio-Rad #1725035). qPCR-reactions were conducted using Sso Advanced
689 Universal SYBR Green Supermix (Bio-Rad #172-5275) on a CFX Connect Real-Time
690 System (Bio-Rad) in 96-well PCR plates (Brand #781366). Experiments for Notch
691 reporter analysis were conducted in biological triplicates and technical duplicates and
692 normalized by *ef1a* and *odc* expression levels. Induction assays were performed in 7
693 biological replicates from 5 different clutches and each with two technical replicates.
694 Expression levels were normalized by *ef1α* and *odc* expression and analyzed in Excel.
695 Graphs were generated using R.

696 qPCR Primer Sequences

Name	**Sequence**
qEf1a-F	CCCTGCTGGAAGCTCTTGAC
qEf1a-R	GGACACCAGTCTCCACACGA
qOdc-F	GGGCTGGATCGTATCGTAGA
qoOdc-R	TGCCAGTGTGGTCTTGACAT
qH2BVenus-F	CACCATCTTCTTCAAGGACGA
qH2BVenus-R	GGCTGTTGTAGTTGTACTCC
qFoxi1-F	TACCAAGAGATGAAGATGATC
qFoxi1-R	CTTGTCAGAAGATAACTGTCCA
qMci-F	AATCAAAAGCATCTGTC
qMci-R	TTTCTTAGAGATTTCCCGCA
qFoxa1-F	GGAGCAACTATTACCAGGAC
qFoxa1-R	ATGGGATTCATAGTCATGTAGG
qTP63DN-F2	AAGCTCTACCTTTGATGCTC
qTP63DN-R2	GATCTGTGGAATACGTCCAG
qFoxj1-F	CCAGTGATAGCAAAAGAGGT
qFoxj1-R	GCCATGTTCTCCTAATGGAT
qHes1-F	TGCGCTCAAGAAAGATAGCTC
qHes1-R	TTACTTCATTCATGCACTCGCT
qHes4-F	GATAAACCCAAGAGTGCCAG
qHes4-R	GTGCTTGACTGTCATTTCCA
qHes5.10-F	CTACAGCAACAGAAGAAACATCAG
qHes5.10-R	CCCACTGTCTCTTTCAAACAC
qHes7.1-F	GAAAGCTATTAAAGCCGTTGGTG
qHes7.1-R	GTGGGAGAAGTTTCCTGGAC
qDll1.L-F	TCACGAACTGAAGAATGAGGA
qDll1.L-R	TTGACGTTGAGTAGGCAGAG
qDlc.s-F	GGCACCTGTATCGAGAAGAG
qDlc.s-R	GACCCATATCTAGACACTGACC
qDll4.L-F	CATCTTTGGCTTGACGTTTCTC
qDll4.L-R	GACTTTCCATTCACCAACATCC
qJag1.L-F	CCAAACCCTGTGTAAATGCC
qJag1.L-R	GCGAAACCCATTAACCAAGTC
qJag2.L+s-F	GATATTTCTGTCACTGCCTTCC
qJag2.L-F	TCTTGCCAATGAAACCACGA
qJag2.s-R	GCTCTATCTCACAATGTTTCCCA

697 Immunofluorescence Staining and Sample Preparation
698 Whole Xenopus embryos, were fixed at indicated stages in 4% paraformaldehyde
699 at 4°C overnight or 2h at room temperature, then washed 3x 15min with PBS, 2x 30min
700 in PBST (0.1% Triton X-100 in PBS), and were blocked in PBST-CAS (90% PBS
701 containing 0.1% Triton X-100, 10% CAS Blocking; ThermoFischer #00-8120) for
702 30min-1h at RT.
703 Mouse anti-Acetylated-α-tubulin (Sigma/Merck #T6793) was used as a primary
704 antibody (1:1000) to mark cilia / MCCs applied at 4°C overnight, AlexaFlour 405-
705 labeled goat anti-mouse antibody (Invitrogen # A30104) was used as a secondary
706 antibody for 2 h at RT (1:250). Both antibodies were applied in 100% CAS Blocking
707 (ThermoFischer #00-8120). Actin was stained by incubation (30-120 min at room
708 temperature) with AlexaFluor 405-labeled Phalloidin (1:800 in PBSt; Invitrogen
709 #A30104), mucus-like compounds were stained by incubation (overnight at 4°C) with
710 AlexaFluor 647-labeled PNA (1:1000 in PBSt; Molecular Probes #L32460).
711
712 Confocal imaging, image processing and analysis
713 Confocal imaging was conducted using a Zeiss LSM880 and Zeiss Zen software.
714 Confocal images were adjusted for channel brightness/contrast, Z-stack projections
715 were generated and cell types were quantified based on their morphology using
716 ImageJ(Schindelin et al., 2012). A detailed protocol for quantification of *Xenopus*
717 epidermal cell types was published(Walentek, 2018) . Images of embryos after *in situ*
718 hybridization and corresponding sections were imaged using an AxioZoom setup or
719 AxioImager.Z1, and images were adjusted for color balance, brightness and contrast
720 using Adobe Photoshop.
721
722 RNA-sequencing on *Xenopus* mucociliary organoids and bioinformatics analysis
723 *X. laevis* embryos were either injected 4x into the animal hemisphere at four-cell
724 stage with mRNAs or MOs or remained uninjected, animal caps were prepared and
725 used for RNA-sequencing at indicated stages. For RNA-seq dataset 1 (cf. **Fig. S2A**),
726 uninjected organoids were collected at st. 9, st. 10.5 (labeled st. 10), st. 11.5 (labeled
727 st. 11) and st. 12.5 (labeled st. 12) and organoids were derived from two independent
728 experiments. For RNA-seq dataset 2 (cf. **Fig. S2A**), organoids were collected at st.
729 10.5 (labeled st. 10), st. 16 (st. 16) st. 25 (st. 25) and st. 32 (st. 32). Organoids were
730 derived from 2 independent experiments. A previously published dataset (*ΔN-tp63*MO
731 RNA-seq, GSE130448; cf. **Fig. S2B**) was used additionally(Haas et al., 2019).
732 500-1000 ng total RNA per sample was used, poly-A selection and RNA-
733 sequencing library preparation was done using non strand massively-parallel cDNA
734 sequencing (mRNA-Seq) protocol from Illumina, the TruSeq RNA Library Preparation
735 Kit v2, Set A (Illumina #RS-122-2301) according to manufacturer's recommendation.
736 Quality and integrity of RNA was assessed with the Fragment Analyzer from Advanced
737 Analytical by using the standard sensitivity RNA Analysis Kit (Advanced Analytical
738 #DNF-471). For accurate quantitation of cDNA libraries, the QuantiFluor™dsDNA
739 System from Promega was used. The size of final cDNA libraries was determined
740 using the dsDNA 905 Reagent Kit (Advanced Bioanalytical #DNF-905) exhibiting a
741 sizing of 300 bp on average. Libraries were pooled and paired-end 100bp sequencing
742 on a HiSeq4000 was conducted at the Transcriptome and Genome Analysis
743 Laboratory, University of Göttingen (RNA-seq dataset 1) or at the Functional
744 Genomics Laboratory, University of California at Berkeley (RNA-seq dataset 2).
745 Sequence images were transformed with Illumina software BaseCaller to BCL files,
746 which was demultiplexed to fastq files with bcl2fastq v2.17.1.14. Quality control was

done using FastQC v0.11.5 (Andrews, Simon (2010). "FastQC a quality-control tool for high-throughput sequence data" available at http://www.bioinformatics.babraham.ac.uk/projects/fastqc).

After adapter-trimming, paired-end reads were mapped to *Xenopus laevis* genome assembly v9.2 using RNA STAR v2.6.0b-1(Dobin et al., 2013). featureCounts v1.6.3(Liao et al., 2014) was used to count uniquely mapped reads per gene and statistical analysis of differential gene expression was conducted in DEseq2 v1.22.1(Love et al., 2014). Heatmaps were generated in R v3.5.1 using ggplot2/heatmap2 v2.2.1. All bioinformatic analysis was performed on the Galaxy / Europe platform (usegalaxy.eu)(Community, 2022).

NGS data generated for this study was deposited at NCBI GEO under the accession numbers GSE215419 (RNA-seq dataset 1) and GSE215373 (RNA-seq dataset 2). Additionally, published data from Haas *et al.* (GSE130448) were used(Haas et al., 2019).

Gene expression plots over time of whole embryos for *hes2.L* and *hes7.1L* (cf. **Fig. 4A**) were generated using Xenbase (http://www.xenbase.org/, RRID:SCR_003280)(Fortriede et al., 2020; Session et al., 2016).

Quantification and statistical evaluation

Stacked bar graphs were generated in Microsoft Excel, box plots (the line represents the median; 50% of values are represented by the box; 95% of values are represented within whiskers; values beyond 95% are depicted as outliers) were generated in R. Heatmaps and Venn diagrams were generated using the Galaxy Europe platform (usegalaxy.eu)(Community, 2022). Sample sizes for all experiments were chosen based on previous experience and used embryos derived from at least two different females. No randomization or blinding was applied.

Use of shared controls

For some of the *in situ* experiments shared controls were used in multiple graphs.

Mathematical modeling

A Notch signaling ODE model for cell fate specification in mucociliary tissue

Our final ordinary differential equation (ODE) model (model 2) consists of 27 dynamical states, 38 reactions, 12 observables, 209 data points and 98 fitted parameters. In the following, it is explained what these quantities represent and how they are linked to each other in the model.

Dynamical states: Molecules and cells

The ODE model elucidates the influence of different molecular compounds on the cell type composition. This implies the model to act on two different scales: the molecular scale on the one hand, the cellular scale on the other. Therefore, unlike most ODE models in systems biology, the 27 dynamical states only partly represent the abundance of molecular compounds. Instead, 7 of them represent cell type abundances (**Table S3** and **S4**).

795 Time evolution of the states

796 The rate equations, which govern the time evolution of system, can be divided
797 into 3 categories:
798

799 1. Rate equations that represent cell state transitions (for simplicity, we still call them
800 "reactions"): Initially, (nearly) all cells start as early progenitors (EPs). In a first step,
801 these early progenitors are assumed to become multipotent progenitors (MPPs) at a
802 constant rate (Reaction 1 in report), i.e. independent from any molecular abundances.
803 This is different in the second step: MPPs themselves turn into ionocytes (ISCs),
804 ciliated cells (MCCs), small secretory cells (SSCs) or basal cells (BCs) based on ΔN-
805 tp63 repression and the effective levels of Hes4, Hes5, Hes7.1 and Spdef. The
806 production rates of ISCs, MCCs, SSCs and BCs are given by hill equations, where
807 each hill equation represents an activating or inhibiting effect from one of the
808 mentioned transcription factors. The precise activations/inhibitions assumed in the
809 model are depicted in the model flow chart (**Fig.S9C**). Most transcription factors act on
810 a cell type either only activating or only inhibiting. The only exception is the effective
811 Spdef level: It activates SSCs at lower levels but inhibits SSCs at higher levels. It was
812 presumed that MPPs have to decide on a cell fate. This is ensured by a prior, that
813 penalizes high MPP abundances compared to BC abundances at a late time point. For
814 MCCs, two different dynamical states are introduced, because the related cell marker
815 *mcidas* is only transiently expressed. The transition from the MCC marker expressing
816 state to the later MCC state is assumed at a constant rate, i.e. independently of
817 transcription factors represented in the model.
818

819 2. Rate equations that represent production and degradation of molecules: All the
820 dynamical states representing molecular abundances (cf. **Table S4**) have a production
821 rate and a degradation rate. The degradation rates are assumed to be proportional to
822 the abundances of all molecular states with individual rate constants. In contrast, the
823 production rate depends on either the molecular abundances or on the cell type
824 composition:
825

826 a.) For all the dynamical states representing RNA (cf. **Table S4**) except the acute
827 Notch level, the production rates depend on other molecular abundances. The
828 precise activation/inhibition connections between the transcription factors are
829 depicted in the model flow chart (**Fig.S9C**). Hes4 is activated for low and
830 inhibited for high effective Notch levels. This is reflected by a product of two hill
831 equations at the according production rate. All others are given by a single hill
832 equation. For all the dynamical states representing protein abundances (cf.
833 **Table S4**), the production rates depend linearly or via a delay chain of length
834 n=4 on the related RNA state.
835

836 b.) The production rate for the acute Notch level depends on the cell composition.
837 It is defined as the weighted mean over the production rates of the individual
838 cell types. The weights are given by the cell type proportions, i.e. the cell type
839 composition. Initially, all the states from **Table S4** are in steady state condition.
840 These steady state conditions are calculated analytically. The starting point of
841 modeling the whole specification process is the transition from EPs to MPPs
842 and the resulting change in cell composition and acute Notch level production.

All other transcription factors are direct or intermediate targets of the acute Notch level.

Embryonic stage representation in the model

The mapping between development stages and physical time in minutes was implemented according to Xenbase.org (http://www.xenbase.org/anatomy/static/xenopustimetemp.jsp). In particular, the values for *Xenopus laevis*, 22°C, average were used. Time point zero (physical time) was chosen to be at stage 9. Stages, where only one sample is present in the weblink table (i.e., where the columns "Average", "Minimum" and "Maximum" coincide), were omitted. The value for the last considered stage, i.e. stage 25, is not present/taken in/from the table, but represents an interpolated value for stage 16 + 8 hours. Values for the physical time are obtained by linear interpolating the values from the columns A and B (**Table S5**).

Link to data

The parameters of the ODE model were fitted by two different types of data: time-resolved RNA-seq TPM data and cell counts from immunofluorescence (IF) images at a single later time of development (st. 32). The RNA-seq data observables (cf. **Table S6**) are linked to the dynamical ODE states via scaling parameters / proportionality factors (cf. **Table S7**), and in some cases offsets (*mcidas, foxa1*). The magnitude of the measurement errors for each observable were fitted by assuming constant error models on the logarithmic scale. The cell count observables for the three specified cell types (ISCs, MCCs, SSCs) coincide with the related dynamical ODE state, i.e. there are no additional parameters in the observation function. Here, measurement errors were taken from the estimated standard deviations over repeated measurements.

Software used

All modelling analyses were conducted using the Data2Dynamics modelling toolbox (https://github.com/Data2Dynamics/d2d)(Raue et al., 2015) which runs under Matlab, The MathWorks, Natick, MA.